EUROPEAN ORGANIZATION FOR NUCLEAR RESEARCH

Study of ^{10}Li via the ^{9}Li(^{2}H,p) reaction at REX-ISOLDE

H.B. Jeppesen[1][2], A.M. Moro[3], U.C. Bergmann[2], M.J.G. Borge[4], J. Cederkäll[2], L.M. Fraile[2], H.O.U. Fynbo[1], J. Gómez-Camacho[3], H.T. Johansson[5], B. Jonson[5], M. Meister[5], T. Nilsson[5][6], G. Nyman[5], M. Pantea[6], K. Riisager[1][2], A. Richter[6], G. Schrieder[6], T. Sieber[7], O. Tengblad[4], E. Tengborn[5] M. Turrión[4] and F. Wenander[2]

Abstract

The ^{9}Li+^{2}H reaction has been investigated at 2.36 MeV/u at the REX-ISOLDE facility. In this paper we focus on the ^{10}Li+p channel which potentially holds spectroscopic information on the unbound nucleus ^{10}Li. The experimental excitation function and angular distribution are compared with CCBA calculations. These calculations clearly support the existence of a low-lying (s) virtual state, with a (negative) scattering length of the order $a_s \sim 13 - 24$ fm and a $p_{1/2}$ resonance with an energy of $E_{\rm res} \simeq 0.38$ MeV and a width of $\Gamma \simeq 0.2$ MeV.

*(Submitted to Physics Letter **B**)*

[1] Institut for Fysik og Astronomi, Aarhus Universitet, DK–8000 Aarhus C, Denmark

[2] ISOLDE, PH Department, CERN, CH-1211 Gen´eve 23, Switzerland

[3] Departamento de FAMN, Universidad de Sevilla, Aptdo. 1065, 41080 Sevilla, Spain

[4] Instituto Estructura de la Materia, CSIC, E-28006 Madrid, Spain

[5] Fundemental Fysik, Chalmers Tekniska Högskola, S-412 96 Göteborg, Sweden

[6] Institut für Kernphysik, Technische Universität Darmstadt,Schlossgartenstr. 9, D-64289 Darmstadt, Germany

[7] Ludwig Maximilians Universität München, Am Coulombwall 1, D-85748 Garching, Germany

1 INTRODUCTION

Spectroscopic information for nuclei along the stability line have successfully been extracted via transfer reactions through the last half century both for bound and unbound states [1, 2]. Now, with the development of low energy (a few MeV/u) radioactive beams, eg. at REX-ISOLDE at CERN and at TRIUMF, this method of extracting spectroscopic information can also be applied to nuclei far off the valley of beta-stability. In this paper we report on the neutron transfer reaction $^9\text{Li}+^2\text{H} \rightarrow ^{10}\text{Li}+\text{p}$ performed in inverse kinematics at the post-accelerator facility REX-ISOLDE at CERN.

The study of the unbound system ^{10}Li is of great interest since knowledge on this system is a necessary ingredient in a theoretical describtion of the halo nucleus ^{11}Li (see eg. [3]). Thompson and Zhukov [4] have, for instance, shown that the presence of a low-lying $s_{1/2}$ virtual state is crucial in order to reproduce the momentum distributions in ^{11}Li fragmentation experiments. Despite the considerable amount of experimental information that has been gathered during the past years, the properties of the continuum of the ^{10}Li system remains unclear, to the extent that the position and spin-parity assignment of the ground state is still controversial. It is widely accepted that the ground state of ^{10}Li is constructed of either a $0p_{1/2}$ or a $1s_{1/2}$ neutron which, coupled to the $3/2^-$ spin of the ^9Li core, would produce states with 1^+, 2^+ or 1^-, 2^- spin assignments, respectively. Theoretically, there are a disparity of predictions. Some calculations suggest that the ground state corresponds to an s-wave [5–7], while others conclude that it should be a p-wave [8, 9]. The existence of an intruder low-lying virtual s-state has been predicted by some theoretical models and is also consistent with the trend observed for the N=7 isotones [10], that predicts a parity inversion in the case of the ^{10}Li nucleus.

Experimentally, the situation is also far from being clear (see [3, 11, 12] and references therein). Although no clear consensus prevails, most results point toward an s-wave ground state and a p-state around 0.5 MeV. The lack of consensus shows the need of experiments to help shed light on the properties of the ^{10}Li nucleus.

2 EXPERIMENTAL SETUP

The experiment was performed at the CERN/ISOLDE facility [13], where a pulsed 1.4 GeV proton beam impinged on a 70 g/cm^2 Ta target, consisting of 13 rolls of 20 μm foils. The produced ^9Li diffused out of the target, into the ion-source and was subsequently accelerated to 30 keV. This low-energy beam was then guided to the REX-ISOLDE post-accelerator [14], were the 1^+ ions where bunched, charge bred to the 2^+ charge state and accelerated to 2.36 MeV/u.

The accelerated ^9Li beam entered the detector setup through a 4 mm collimator before it impinged on the reaction target; 6.4 μm (660 μg/cm^2) of deuterated polyethylene (C$_3$D$_6$ with approximately 3% H contamination). The reaction products were detected with two telescopes: One small three-layered telescope (10, 300 and 700 μm Si) of 10×10 mm^2 area situated at 45° scattering angle covering about 15°. The second telescope consisted of a 16×16 strip Double Sided Silicon Strip Detector (DSSSD) of 50×50 mm^2 area backed by a 1000 μm Si-pad detector of the same area. The DSSSD was of 64 μm thickness, which allowed protons with more than 2.5 MeV to go through the DSSSD and into the back detector, thus allowing particle identification. The DSSSD telescope covered laboratory angles from 18° to 80°.For a more elaborate description of the experimental setup and analysis method see [15–17].

3 CALCULATIONS

Since ^{10}Li is unstable against neutron emission, the $^9\text{Li}(^2\text{H,p})^{10}\text{Li}$ reaction populates states in the n+^9Li continuum. Spectroscopic analysis of transfer reaction leading to unbound states rely

on the assumption that the structures in the measured excitation function contain information on the properties of the final nucleus. Furthermore, it is commonly assumed that the energy and width of the peaks in this excitation function correspond to the position and width of the resonances. These parameters are obtained by means of an R-matrix fit of the experimental excitation function in which resonances are typically parametrized in terms of Breit-Wigner line shapes. This procedure is indeed justified if the excitation function is not significantly affected by the reaction mechanism and final state interactions.

In this work we adopt a different procedure. Instead of extracting the resonance parameters from a fit of the data, we will treat the reaction within the coupled-channels Born approximation (CCBA) formalism [1], conveniently adapted for unbound final states [18]. Using this approach the reaction mechanism as well as the continuum structure of the ^{10}Li nucleus enter in a consistent way, without any *a priori* assumption about position or shape of the peaks in the excitation function. Although the CCBA method for the case of unbound states is formally similar to the case of final bound states, there are, however, some important differences between the two situations. In transfer reactions populating bound states, only discrete values of the energy and angular momenta in the final nucleus are permitted. By contrast, in transfer reactions to the continuum, any excitation energy and angular momentum is allowed. Nevertheless, as we will see below, at this bombarding energy only excitation energies below $E_x \approx 1$ MeV and small relative angular momenta in the n+^{9}Li system are significantly populated, thus greatly simplifying the calculations and the interpretation of the results. Another important difference comes from the fact that scattering states are non-normalizable, leading to convergence problems in the evaluation of the transition amplitude [19]. To overcome this difficulty a discretization procedure was used in order to represent the two-body continuum of the n+^{9}Li system by a discrete set of normalizable states. With this procedure, the conventional expressions for the transition amplitude can be evaluated in exactly the same way as for bound states. In the present analysis, we treat the transfer process within the Born approximation, but we include all couplings between all final states considered in the calculation. In particular, we used the prior representation of the transition matrix which, in the present case, involves the matrix element of the operator $V_{[\text{n}-^9\text{Li}]} + U_{[\text{p}-^9\text{Li}]} - U_{[\text{d}-^9\text{Li}]}$. The entrance channel optical potential, $U_{[\text{d}-^9\text{Li}]}$, was taken from the fit of the elastic data performed in [16]. For the core-core interaction, $U_{[\text{p}-^9\text{Li}]}$, we used the proton optical potential of Powell *et al.* [20]. The exit channel potential, $U_{[\text{p}-^{10}\text{Li}]}$, was constructed from the folding of the p–n and p–^{9}Li interactions. For the former, we used the Gaussian parametrization $V(r) = -V_0 \exp[-r^2/a^2]$, with V_0=72.15 MeV and $a = 1.484$ fm, which reproduces the deuteron binding energy and rms radius. Both diagonal and non-diagonal couplings were included. In the present calculations, only $\ell = 0, 1$ orbital angular momenta are considered for the neutron-^{9}Li relative motion. The s- and p-wave interactions were chosen in order to reproduce the known properties of the ^{10}Li continuum. In this nucleus, the lowest $s_{1/2}$ state must be bound. The properties of the low-energy $\ell = 0$ continuum are related to the presence of a non-normalizable, exponentially increasing virtual state with small negative energy. The $p_{3/2}$ level is bound by about 4.1 MeV, while the $p_{1/2}$ wave gives rise to a low-lying resonance.

Following the work of Garrido *et al.* [3], the s and p components of the n-^{9}Li interaction are represented by Gaussian shapes. In both cases, the radius was fixed to $a = 2$ fm, which gives a rms radius for ^{9}Li of 2.32 fm [3], in good agreement with the experimental value. For the $\ell = 0$ wave, we varied the potential depth in the range V_s=90–102 MeV. For any value within this range, this potential supports a deeply bound $0s$ state and a $1s$ virtual state, whose position depends on the particular choice of V_s. The range of values considered here
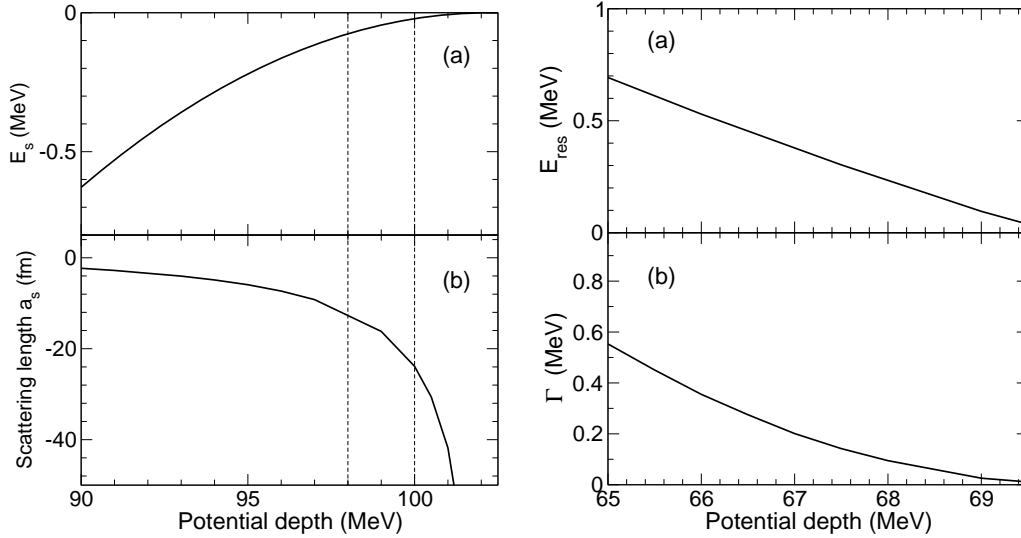
Fig. 1: Left: position (in MeV) of the $s_{1/2}$ virtual state (upper panel) and scattering length (lower panel) as a function of the potential depth. Right: position and width of the $p_{1/2}$ resonance as a function of the potential strength. In both cases, the ^{9}Li+n potential corresponds to a Gaussian with potential radius a =2 fm. The scattering length was calculated from the elastic phase-shift by means of the formula $a_s = -\lim_{k\to 0} \tan \delta_0(k)/k$. The dashed vertical lines delimit the range of values which provide acceptable fits of the measured excitation function for the s virtual state.

is compatible with the existence of a virtual state below 1 MeV (see Fig. 1). For $V_s > 102.3$ MeV the potential contains a second bound s-state ($2s$) which is not present in ^{10}Li. In order to reproduce the splitting of the $p_{1/2}$ and $p_{3/2}$ doublet, the $\ell = 1$ potential included also a spin-orbit term. As in [3], the radial dependence of the spin-orbit potential is also parametrized using a Gaussian shape, with the same range as that of the central potential. The total strength of the $p_{1/2}$ potential (which includes the central and spin-orbit components) is then varied in order to generate a resonance at the desired excitation energy. In this work, the position of the resonance is defined as the energy at which the n+^{9}Li elastic phase-shift crosses $\pi/2$. In our analysis, we considered potential depths within the range 65–70 MeV which, according to the criterion above, is consistent with the existence of a resonance in the energy range $E_x \simeq 0.05 - 0.7$ MeV (see Fig. 1). Once the position of the resonance has been obtained, the width is calculated from the $p_{1/2}$ phase-shifts as $2/\Gamma = d\delta_k/dE_x$ ([21] p. 96), where the derivative is evaluated at the energy of the resonance.

Then, we discretize the $\ell = 0$ and $\ell = 1$ continua from zero to $E_{\max} = 1.5$ MeV into energy bins of 0.1 MeV and 0.05 MeV, respectively. For $\ell = 1$ we used a finer discretization for a better description of the resonance peak. For the states with $\ell = 1$, only the $p_{1/2}$ continuum was included, since the contribution to the cross section coming from the states with $p_{3/2}$ was found to be very small. This is expected since, in a mean field description of the ^{10}Li nucleus, the $0p_{3/2}$ orbit is bound and fully occupied and the next (unbound) $p_{3/2}$ states would arise from the next oscillator shell ($1p_{3/2}$), which lies at much higher energies. The coupled equations were integrated up to a maximum total angular momentum of $J_{\max} = 8$ and with a matching radius of 200 fm. This large radius is motivated by the extension of the continuum bins. The range of the non-local kernels, which arise from the transfer couplings, was set to 16 fm. These calculations were performed with the computer code FRESCO [22], version frxy.3d.
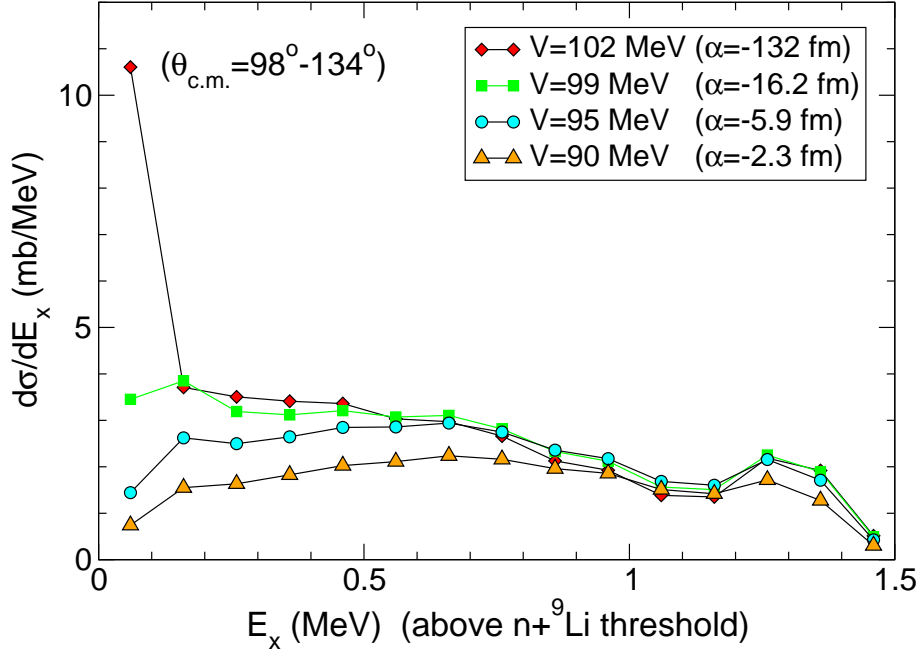
4

Fig. 2: (Color online) Calculated excitation function for ^{9}Li(^{2}H,p)^{10}Li leading to $\ell = 0$ states in the ^{10}Li ($=^9$Li+n) system. The x-axis corresponds to the excitation energy in the ^{10}Li system. The ^{9}Li+n potential corresponds to a Gaussian with potential radius $a =2$ fm, and depths indicated by the labels.

We first study the separate contribution of the $s_{1/2}$ and $p_{1/2}$ waves to the excitation functions. For this purpose we performed CCBA calculations including either the $s_{1/2}$ or the $p_{1/2}$ states. In both cases, all continuum-continuum couplings (diagonal and non-diagonal) were included. In Fig. 2 we present the calculated energy distributions arising from $s_{1/2}$ states in ^{10}Li, integrated over the angular range covered by the experiment ($\theta_{c.m.}$=98°–134°), and for different depths of the neutron-^{9}Li potential (labelled by the scattering length). Except for the case V_s=102 MeV, these distributions exhibit a broad structure, with a maximum that appears roughly at the energy of the virtual state, with opposite sign. It can be seen that the cross section is particularly favoured when the virtual state approaches zero energy. In particular, for V_s=102 MeV (which is very close to the limit case $V_s = 102.3$ MeV, where the virtual state becomes bound) the cross section is greatly enhanced at zero energy. The calculations also show a small bump at high energies, regardless of the position of the virtual state.

In Fig. 3 we present the contribution of the $p_{1/2}$ wave to the energy differential cross section, for three different values of the potential strength, which correspond to different positions of the resonance, as indicated by the labels. Note that, unlike the $\ell = 0$ case, the $p_{1/2}$ cross section drops rapidly when the excitation energy approaches zero. This is in fact a general property of $\ell \neq 0$ waves. As discussed below, this feature has important consequences regarding the interpretation of the low-lying strength observed in the experimental data (see Fig. 5). The $p_{1/2}$ distribution has a well defined maximum at an energy which is very close to the resonance position. When the depth of the n+^{9}Li potential increases, the $p_{1/2}$ resonance moves to lower energies and becomes narrower (see Fig. 1). Correspondingly, the position of the calculated peak in the excitation function is also shifted to smaller excitation energies and the bump becomes narrower. Therefore, there is a clear correspondence between the resonance parameters and the observed peak in the excitation function. Note that, in general, the observed width may
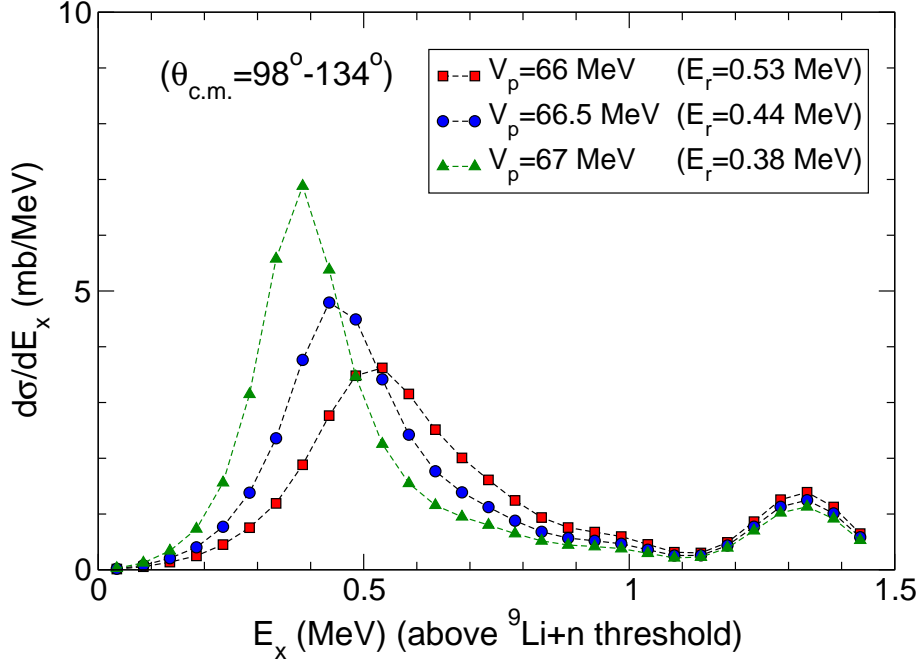
Fig. 3: Calculated excitation function for the reaction $^9\text{Li}(^2\text{H},p)^{10}\text{Li}$ leading the $\ell = 1$ ($p_{1/2}$) states in the ^{10}Li ($=^9\text{Li}+n$) system. The abscissas corresponds to the excitation energy in the ^{10}Li system above the neutron-^9Li threshold.

differ from the true resonance width due to the influence of the reaction mechanism and also to experimental resolution, which is taken into account in our calculations. Our predictions for the $\ell = 0$ and $\ell = 1$ breakup are qualitatively similar to those found by Blanchon *et al.* [23], where calculations for this reaction were performed using the semiclassical transfer to the continuum approach.

In Fig. 4 we compare the experimental data with a best fit analysis of the theoretical excitation function. The depths V_s and V_p where varied independently in order to minimize the chi square. With this procedure we obtained the potential strengths V_s=100 MeV (virtual state at $|E_x| \simeq 22$ keV with scattering length $a_s = -23.9$ fm) and V_p=67 MeV (resonance at $E_x \simeq 0.38$ MeV and width $\Gamma = 0.20$ MeV). All continuum couplings (s–s, p–p and s–p) were included in the calculations. For a reliable comparison with the data all the theoretical curves have been folded with the experimental energy acceptance for the detected protons. Moreover, in the calculations we adopted the same binning scheme used for the experimental data. In Fig. 4 the dashed and thin solid lines correspond to the calculated $s_{1/2}$ and $p_{1/2}$ contributions, respectively. The thick solid line is the sum of these two curves. It can be seen that this calculation reproduces very well the shape of the experimental data, although the absolute normalization is somewhat underestimated. This underestimation could be due to the contribution of other continuum configurations not considered in our calculation, to the evaporated protons or even to the uncertainties associated with the calculations, such as the potential parameters. Note also that the small bump observed in the calculated $s_{1/2}$ and $p_{1/2}$ distributions at excitation energies around 1.3 MeV (see Figs. 2 and 3) disappears in the smoothed calculation, due to the small detection efficiency of low energy protons. It is clearly seen that the contribution of the $s_{1/2}$ wave is essential to describe the low energy part of the spectrum. Therefore, our calculations clearly support the existence of a low-lying virtual state, as found by other authors [12, 24–26].
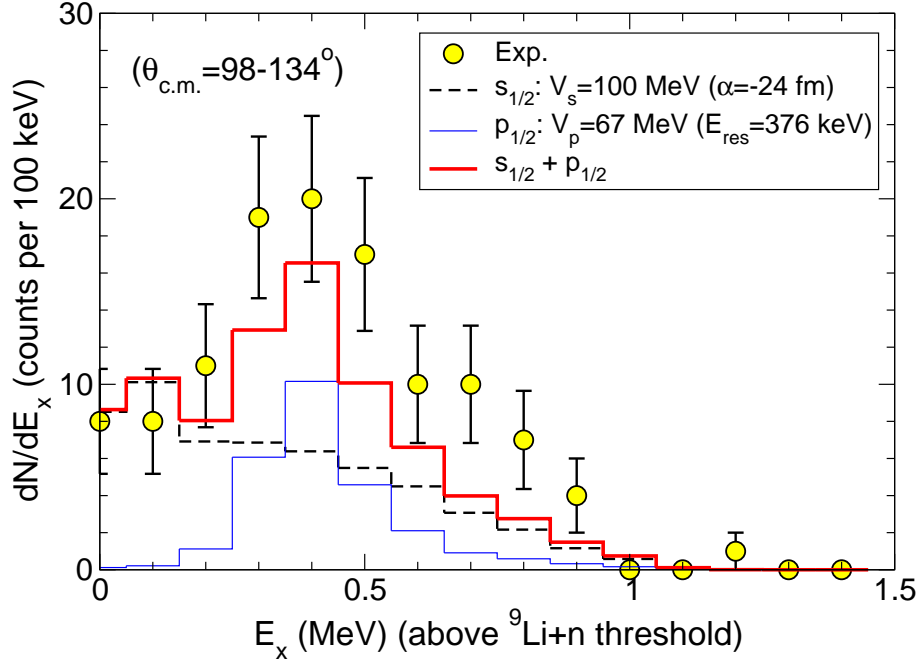
Fig. 4: (Color online) Relative contribution of $s_{1/2}$ and $p_{1/2}$ final states in the ^{9}Li+n system to the excitation function for the reaction ^{9}Li(^{2}H,p)^{10}Li.

As for the $p_{1/2}$ contribution (thin solid line in Fig. 4), it is found to be crucial to describe the peak at $E_exp \sim 0.4$ MeV. Calculations including the d-waves were also performed, but the effect on the observables was found to be very small. Therefore, we conclude that this reaction proceeds mainly via the population of the $s_{1/2}$ and $p_{1/2}$ states in the n+^{9}Li system.

In the chi square analysis, we found that reasonable fits of the data can be obtained with s strengths within the range $V_s \simeq 98 - 100$ MeV. This corresponds to a virtual s state around $|E_s| = 22 - 76$ keV with a (negative) scattering length of magnitude $|a_s| = 13 - 24$ fm (see Fig. 1). For $V_s > 100$ MeV the cross section grows rapidly at zero energy, in contrast to the observed behaviour.

Our estimate for the position of the p resonance is consistent with the value reported by Santi *et al.* [27], $E_r = 0.35 \pm 0.11$ MeV, which was obtained from the analysis of the ^{9}Li(^{2}H,p)^{10}Li reaction at 20 MeV/nucleon. It is worth to note that some authors have also found evidences for a second p resonance at lower energies (~ 240 keV). For example by Santi *et al.* [27] where the measured excitation function could also be well described in terms of two resonances at 0.2 and 0.77 MeV, which could not be determined as either s- or p-waves.

In the present experiment with an energy resolution of ~ 300 keV in the (^{9}Li+n) excitation energy spectrum we can clearly see that the peak in ^{10}Li is not composed of two peaks at 0.2 and 0.77 MeV. It is worth to note that, once the geometry of the neutron-^{9}Li potential is fixed, one can not vary independently the energy and width of the resonance in order to improve the fit of the data. A similar argument applies to the $s_{1/2}$ virtual state, whose parameters (position and scattering length) are completely determined by the V_s potential. Therefore, our fits are obtained with only two free parameters, namely, the scattering length (or energy) of the $s_{1/2}$ virtual state and resonance position (or width) of the $p_{1/2}$ resonance.

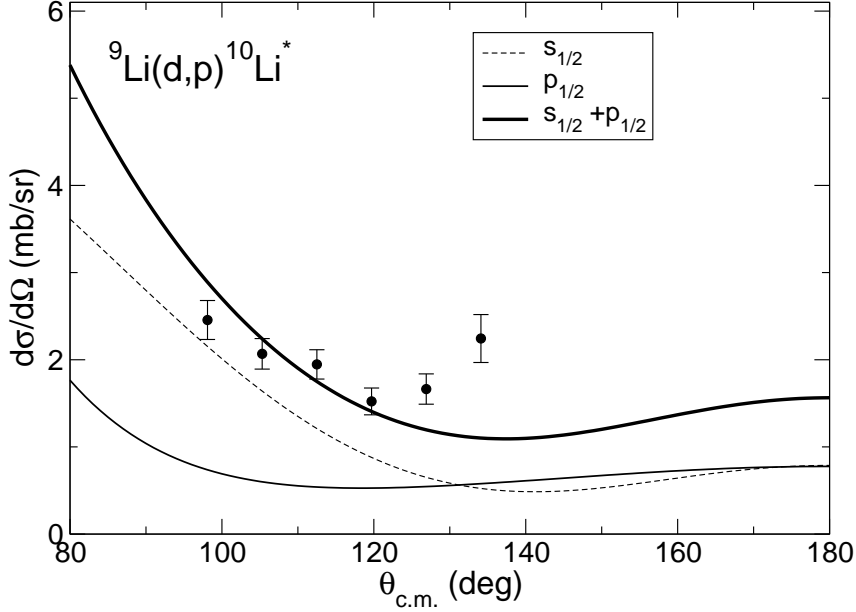Besides the excitation functions, experimental angular distributions for the outgoing protons

Fig. 5: Relative contribution of $s_{1/2}$ and $p_{1/2}$ final states in the ^{9}Li+n system to the proton angular distribution.

were also obtained. These data are represented in Fig. 5 (solid circles), and compared with the CCBA calculation. The $s_{1/2}$ and $p_{1/2}$ contributions are represented by the dashed and thin solid lines, respectively. The thick solid line is the sum of these two components. Except for the last point, the calculation reproduces reasonably well the shape and normalization of the data.

4 SUMMARY AND CONCLUSIONS

In this work, new experimental data for the ^{9}Li(^{2}H,p)^{10}Li reaction has been obtained at the REX-ISOLDE facility. From the measured energy and angular distribution of the detected protons, the excitation function and angular distribution of the ^{10}Li system have been reconstructed.

These observables have been compared with CCBA calculations in which the final states correspond to different angular and energy configurations of the neutron-^{9}Li system. In order to deal with normalizable final states, the continuum spectrum of the ^{10}Li nucleus was discretized into energy bins. We found that, at these energies, this reaction populates states of the n+^{9}Li system at low excitation energies, and small relative angular momentum. In particular, we have shown that the energy spectrum can be very well described including $\ell = 0$ and $\ell = 1$ waves only. The inclusion of the $\ell = 0$ virtual state with a negative scattering length of the order of 13–24 fm was essential in order to reproduce the observed strength at low energy.

At higher excitation energies, the spectrum is dominated by the contribution of the $p_{1/2}$ resonance. This resonance is in fact responsible for the observed peak in the excitation function at $E_x \simeq 0.4$ MeV. Our calculations show that the energy of the peak coincides with the position of the resonance in the neutron-^{9}Li system. This is an important result, because it clearly indicates that it is possible to establish a simple correspondence between the position of the resonance in the ^{10}Li system from the position of the maxima in the energy spectrum. According to our potential model for the n+^{9}Li system, the width of the $p_{1/2}$ resonance is $\Gamma \approx 200$ keV.

Finally, we emphasize that the present method does not make any *a priori* assumption on the shape of the excitation function and, moreover, does not require any arbitrary normalization

factor. Also, resonant and non-resonant continua are included consistently.

This work shows that the measurement of reactions involving simple reaction mechanisms, combined with the application of fundamental direct reaction theories is a powerful tool to obtain reliable spectroscopic information of unbound nuclei.

REFERENCES

[1] G. R. Satchler, Direct Nuclear Reactions, Oxford University Press, New York, 1983.

[2] P. E. Hodgson, Nuclear reactions and nuclear structure, Clarendon Press, Oxford, 1971.

[3] E. Garrido, D. V. Fedorov, A. S. Jensen, Nucl. Phys. A 700 (2002) 117–141.

[4] I. Thompson, M. V. Zhukov, Phys. Rev. C 49 (1994) 1904.

[5] F. C. Barker, G. T. Hickey, J. Phys. G 3 (1977) L23.

[6] B. A. Brown, Proceedins of the International Conference on Exotic Nuclei and Atomic Masses, Arles France (1995) 451.

[7] N. A. F. M. Poppelier, A. A. Wolters, P. Glaudermans, Z. Phys. A 346 (1993) 11.

[8] J. Wurzer, H. M. Hofmann, Z. Phys. A 354 (1996) 135.

[9] H. G. Bohlen et al, Z. Phys. A344 (1993) 381.

[10] P. G. Hansen, Nucl. Phys. A 630 (1998) 285.

[11] J. A. Caggiano et al, Phys. Rev. C 60 (1999) 064322.

[12] M. Thoennessen et al, Phys. Rev. C 59 (1999) 111.

[13] E. Kugler, Hyp. Int. 129 (2000) 23.

[14] D. Habs, Hyp. Int. 129 (2000) 43.

[15] H. B. Jeppesen, PhD thesis, University of Aarhus, unpublished .

[16] H. B. Jeppesen et al, Nucl. Phys. A 748 (2005) 374.

[17] H. B. Jeppesen et al, Phys. Lett. B 635 (2006) 17.

[18] A. M. Moro, R. Crespo, H. García-Martínez, E. F. Aguilera, E. Martínez-Quiroz, J. Gómez-Camacho, F. M. Nunes, Phys. Rev. C 68 (2003) 034614.

[19] C. M. Vincent, H. T. Fortune, Phys. Rev. C 2 (1970) 782.

[20] D. L. Powell, G. M. Crawley, B. V. N. Rao, B. A. Robson, Nucl. Phys. A 147 (1970) 65.

[21] C. J. Joachain, Quantum collision theory, North-Holland, 1987.

[22] I. J. Thompson, Comp. Phys. Rep. 7 (1988) 167.

[23] G. Blanchon, A. Bonaccorso, N. V. Mau, Nucl.Phys. A 739 (2004) 259.

[24] M. Zinser et al, Phys. Rev. Lett. 75 (1995) 1719.

[25] S. N. Abramovich, B. Ya Guzhovskii, L. M. Lazarev, Phys. Part. Nucl. 26 (1995) 423.

[26] M. Chartier *et al.*, Phys. Lett. B 510 (2001) 24.

[27] P. Santi *et al.*, Phys. Rev. C 67 (2003) 024606.